Intermediate Zonal Jets in the Tropical Pacific Ocean Observed by Argo Floats*

SOPHIE CRAVATTE

LEGOS, Université de Toulouse (OMP-PCA)/IRD/CNRS/CNES, and Institut de Recherche pour le Développement, LEGOS, Toulouse, France

WILLIAM S. KESSLER

National Oceanic and Atmospheric Administration/Pacific Marine Environmental Laboratory, Seattle, Washington

FRÉDÉRIC MARIN

LEGOS, Université de Toulouse (OMP-PCA)/IRD/CNRS/CNES, Toulouse, France, and Institut de Recherche pour le Développement, LEGOS, Nouméa, New Caledonia

(Manuscript received 8 November 2011, in final form 25 January 2012)

ABSTRACT

Argo float data in the tropical Pacific Ocean during January 2003–August 2011 are analyzed to obtain Lagrangian subsurface velocities at their parking depths. Maps of mean zonal velocities at 1000 and 1500 m are presented. At both depths, a series of alternating westward and eastward zonal jets with a meridional scale of 1.5° is seen at the basin scale from 10°S to 10°N. These alternating jets, with mean speeds about 5 cm s^{-1}, are clearly present in the western and central parts of the basin but weaken and disappear approaching the eastern coast. They are stronger in the Southern Hemisphere. Along the equator at both 1000 and 1500 m, a westward jet is seen. The jets closer to the equator are remarkably zonally coherent across the basin, but the jets farther poleward appear broken in several segments. In the western half of the basin, the 1000-m zonal jets appear to slant slightly poleward from east to west. At the western boundary in the south (east of Solomon Islands and Papua New Guinea), the alternating jets appear to connect in narrow boundary currents. Seasonal zonal velocity anomalies at 1000 and 1500 m are observed to propagate westward across the basin; they are consistent with annual vertically propagating Rossby waves superimposed on the mean zonal jets. Their meridional structure suggests that more than one meridional mode is present.

1. Introduction

The equatorial oceans play an important role in our climate system and in the general circulation of the world's oceans. The upper structure of the equatorial Pacific has been extensively observed and has received much attention for its relation with the El Niño–Southern Oscillation phenomenon. However, observations of middepth currents below 400 m are sparse and synoptic, and there remain large gaps in our knowledge and understanding of the subthermocline currents.

Firing (1987) and Gouriou et al. (2006) presented observed synoptic meridional sections of deep currents in the western equatorial Pacific. They showed evidence of a series of westward and eastward jets from 3°S to 3°N (Firing 1987), and from the equator to 10°S (Gouriou et al. 2006), with large vertical extent, alternating every 1.5°–2° in latitude, with amplitudes of about 10 cm s^{-1}. Firing et al. (1998), comparing meridional sections at different longitudes from 3°S to 3°N, provided evidence that these jets are zonally coherent over a large portion of the equatorial Pacific, as later observed by Ascani et al. (2010). Their meridional location appears to remain the same across the basin. Nevertheless, Firing et al. (1998) pointed out that nothing is known about what happen to them at the boundaries.

* Pacific Marine Environmental Laboratory Contribution Number 3777.

Corresponding author address: Sophie Cravatte, IRD, LEGOS, 14 avenue Edouard Belin, Toulouse 31400, France.
E-mail: sophie.cravatte@ird.fr

DOI: 10.1175/JPO-D-11-0206.1

The present state of knowledge of these subthermocline jets near 1000 m in the Pacific can be described as follows: On the equator, the mean lower equatorial intermediate current (LEIC) is westward but reverses seasonally (Gouriou et al. 2006; Marin et al. 2010). Below the LEIC's core, equatorially confined jets alternating in the vertical every 200 m, the so-called equatorial deep jets, complicate the picture (e.g., Firing 1987; Johnson et al. 2002). The eastward South Intermediate Countercurrent (SICC) and North Intermediate Countercurrent (NICC) are centered around 1.5°–2°S and 1.5°–2°N. At 3°S, the South Equatorial Intermediate Current (SEIC) flows westward; its northern counterpart, the North Equatorial Intermediate Current (NEIC), has been less firmly observed, but its existence has been suggested at several longitudes (Firing et al. 1998). Around 5°S, Gouriou et al. (2006) observed an eastward current that they identified as the deep extension of the secondary Tsuchiya Jet described by Rowe et al. (2000). The vertical extent of all these jets is not known, but observations from Firing et al. (1998) suggest that the NICC, extending from about 500 to 1000 m, is shallower than the southern SICC and SEIC. Poleward of 6°S and 3°N, little is known about the existence of subthermocline zonal currents. Their mean structure, variability, and dynamics are largely unknown.

Any new observation is thus potentially valuable to expanding our knowledge. Following successful previous attempts in the Atlantic Ocean that used both acoustic and profiling floats (Ollitrault et al. 2006), this note takes advantage of Argo float drifting velocities. Davis (1998, 2005) presented observations of middepth currents objectively mapped from autonomous float drifts (pre-Argo) in a manner similar to what is done here; however, the sampling density at that time was insufficient to resolve the narrow features that can now be seen. We present maps of the mean structure of zonal jets in the equatorial Pacific at the Argo parking depths of 1000 and 1500 m. We show their connections near the southwestern equatorial Pacific boundary (the Solomon Islands and Papua New Guinea). The Argo velocities provide a description of the meridional, zonal, and vertical extension of these jets and their seasonal variability.

2. Data

Argo float data from January 2003 to August 2011 were analyzed to obtain a Lagrangian subsurface velocity corresponding to the drift of each float at its parking depth. A total of 895 floats entering the 12°S–12°N, 120°E–80°W region were analyzed, with 89% of them being post-2005. At typically 10-day intervals, the floats descend to 2000 m and rise to the surface over about 6 h while measuring temperature and salinity. Satellites determine the position of the floats when they surface. A float typically spends 6–12 h at the surface. Then, it dives again to its parking depth and drifts about 9 days until the cycle is repeated. We used the positions and time of transmissions before and after each dive to compute the subsurface and surface velocities, following Park et al. (2005). Then, each float's trajectory and the parameters of its dive were visually inspected to eliminate obvious bad values (around 8% of the dives). This dive-by-dive checking, while time consuming, is essential as many apparent inconsistencies were found and removed.

Most of the floats (73%) have a parking depth around 1000 m (Fig. 1). However, some have deeper or shallower parking depths: 18% drift around 1500-m depth. We considered only the Argo floats drifting at depths between 950 and 1050 m and those drifting between 1450 and 1550 m, and we treated them separately.

Sources of errors in the subsurface velocity computation were considered. Each float spends some time at the surface before it makes its first transmission and does not actually leave the surface until some time after the last transmission. Therefore, the actual surface drift is larger than would be computed from the positions and time transmitted by the float. If we assume 4 h of unsampled surface drift, the resulting error is relatively small: its median value is estimated at 0.35 cm s^{-1} and its 90% quantile is 0.9 cm s^{-1}. During its dive, the float also drifts because of subsurface currents encountered between the surface and its deepest position. Computing the geostrophic velocity shear from the Commonwealth Scientific and Industrial Research Organisation (CSIRO) Atlas of the Regional Seas (CARS2009) (Condie and Dunn 2006), we estimated this error and found it also small: its median value is 0.4 cm s^{-1} and its 90% quantile is 1 cm s^{-1}. We chose not to apply any additional correction to the subsurface velocities, because applying corrections did not change our results significantly and potentially added an unknown source of uncertainty.

Then, Lagrangian zonal and meridional velocities at 1000 and 1500 m were gridded independently to produce a monthly climatological field on a 1° longitude × 0.25° latitude grid, using an optimal objective analysis method (De Mey and Menard 1989). This method, applied to a 3D base (x, y, t), gives a value of subsurface velocity at each grid point, using nearby data only. Around each grid point, data are mapped taking into account the spatial and temporal scales of the relevant dynamics. The decorrelation scales used were 3 months (to resolve the seasonal cycle), 330 km in the zonal direction (the best compromise to slightly smooth the jets while keeping estimates independent every 6° of

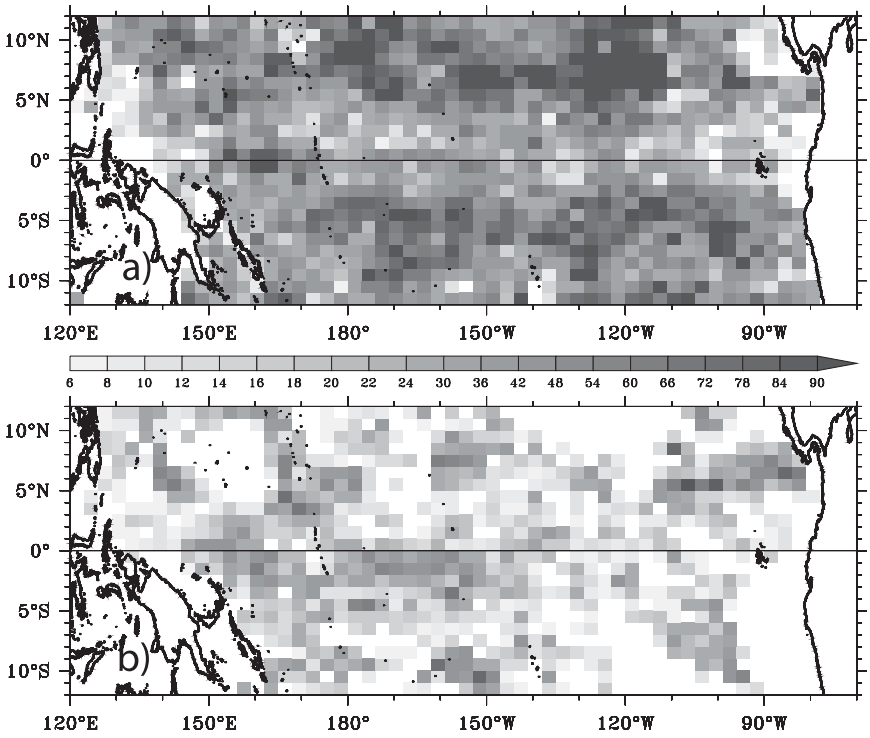

FIG. 1. Number of subsurface velocities data in 3° × 1° boxes for (a) floats drifting between 950 and 1050 m and (b) floats drifting between 1450 and 1550 m, for the period January 2003–August 2011.

longitude) and 55 km in the meridional direction, to correctly resolve the small meridional scale of the jets. Near the western coast (and in Fig. 5), the data were gridded each 0.25° in longitude and the longitudinal decorrelation radius was reduced to 110 km. These empirical scales have been chosen a posteriori. It is noteworthy that the gridding method gives, in addition to the interpolated velocities, a normalized error at each grid point, allowing us to estimate the confidence we can place in the jets we observe. Only data for which the error is less than 60% of the variance are used. These monthly errors are also used to estimate the possible seasonal bias that could alias into the zonal velocity mean. If the zonal velocity estimate error is less than 60% of the variance at least once during each of the four different seasons [December–February (DJF), March–May (MAM), June–August (JJA), and September–November (SON)], we consider that our mean estimate is statistically significant. If not, the mean may be biased seasonally, and the gridpoint is hatched in Fig. 2.

The number of subsurface velocity samples at 1000 and 1500 m in each 3° × 1° grid box is plotted in Fig. 1. At 1000 m, most of the tropical Pacific is well sampled, except south of the Halmahera eddy (0°–4°N, 130°–140°E), in the Bismarck Sea, and east of the Galapagos Islands. However, at 1500 m, large regions remain unsampled. This paper thus focuses on the 1000-m velocities and uses the 1500-m velocities to discuss the deeper extension of the jets.

3. Equatorial intermediate zonal jets

a. Mean structure of the jets at 1000 m

The zonal velocity by far dominates the meridional velocity in most locations (not shown), except near the western boundary (Fig. 5). Therefore, Figs. 2a and 3a show the mean zonal currents at 1000 m and their zonal average, respectively. Several features stand out:

- The zonal velocity at 1000 m is dominated by alternating westward and eastward jets with a meridional scale of 1.5° and speeds about 5 cm s^{-1}.
- The jets are strong in the western and central parts of the basin but weaken and eventually disappear in the east (near 110°W at the equator, farther west poleward).
- The jets are stronger in the Southern Hemisphere, where six to seven jets can be identified at 1000 m. They are weaker (except in the west) in the Northern Hemisphere, where seven to eight jets are also

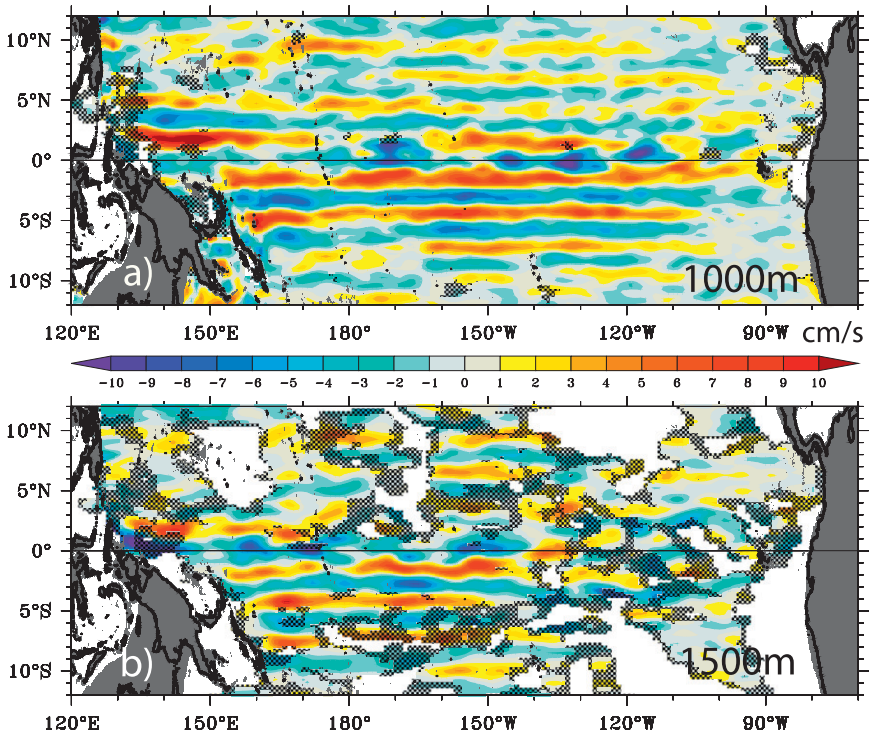

FIG. 2. Mean zonal currents (cm s^{-1}) at (a) 1000 and (b) 1500 m, from optimal interpolation. Topography shallower than 1000-m depth is shaded in dark gray. Boxes with less than five values are blanked. Regions where zonal velocity estimates could be biased seasonally are hatched in black (see text in section 2).

identified, but their meridional positions and amplitudes appear less constant across the basin.

- In the western Pacific, the 1000-m zonal jets appear to slant slightly poleward from east to west.

These in situ observations with global coverage show the existence of mean zonally coherent middepth zonal jets at 1000 m across the entire basin, confirming and extending the synoptic observations of Firing et al. (1998). Moreover, these jets are observed from 10°S to 10°N, a much wider latitudinal range than shown by previous observations.

Noting the regular meridional oscillations of zonal currents in Fig. 3a, it appears that the individual jets are part of a system of alternating eastward and westward zonal currents, whose characteristics are relatively similar across a region much broader than the meridional scale of the jets themselves. Therefore, we chose to use complex demodulation (CD) in the meridional direction to describe the positions of the jets more precisely and to quantify the observations listed above. Complex demodulation (Bloomfield 1976; Kessler et al. 1995) is a bandpass filtering technique that expresses local (slowly varying) amplitude, phase, and wavelength of a nearly periodic signal oscillating around a central frequency. We performed the demodulation at each longitude separately, choosing a central wavelength of 3° of latitude. The results of the method were found not to be sensitive to this central wavelength choice. At each longitude, the filtered currents can be reconstructed using $u(y) = A(y)\cos[\omega y + \phi(y)]$, where A (cm s^{-1}) is the amplitude, ϕ is the phase, and ω ($2\pi/3°$ latitude) is the central frequency (wavenumber). The reconstructed currents are shown in Fig. 4a, and their zonal average is superimposed on the mapped currents in Fig. 3a, demonstrating the appropriateness of the method. The locations of eastward and westward jet maxima of the filtered currents are shown in Fig. 3b.

At the equator, the LEIC flows westward from about 110°W to the western boundary (Fig. 4a). It appears noisy, with local maxima of more than 10 cm s^{-1} and local positive minima, apparently due to limited sampling at some longitudes. At 1.5°S, the eastward SICC is seen from east of New Ireland to the Galapagos Islands. Its meridional position stays remarkably constant, as well as its mean amplitude of 6 cm s^{-1}. Its northern counterpart, the NICC, flows eastward at 1.5°N from Halmahera to about 100°W. It is stronger and slightly farther north in the western part of the basin (about 8 cm s^{-1}) and weaker in the central and eastern part (about 4 cm s^{-1}). It also appears broken up into several segments and less continuous than the SICC.

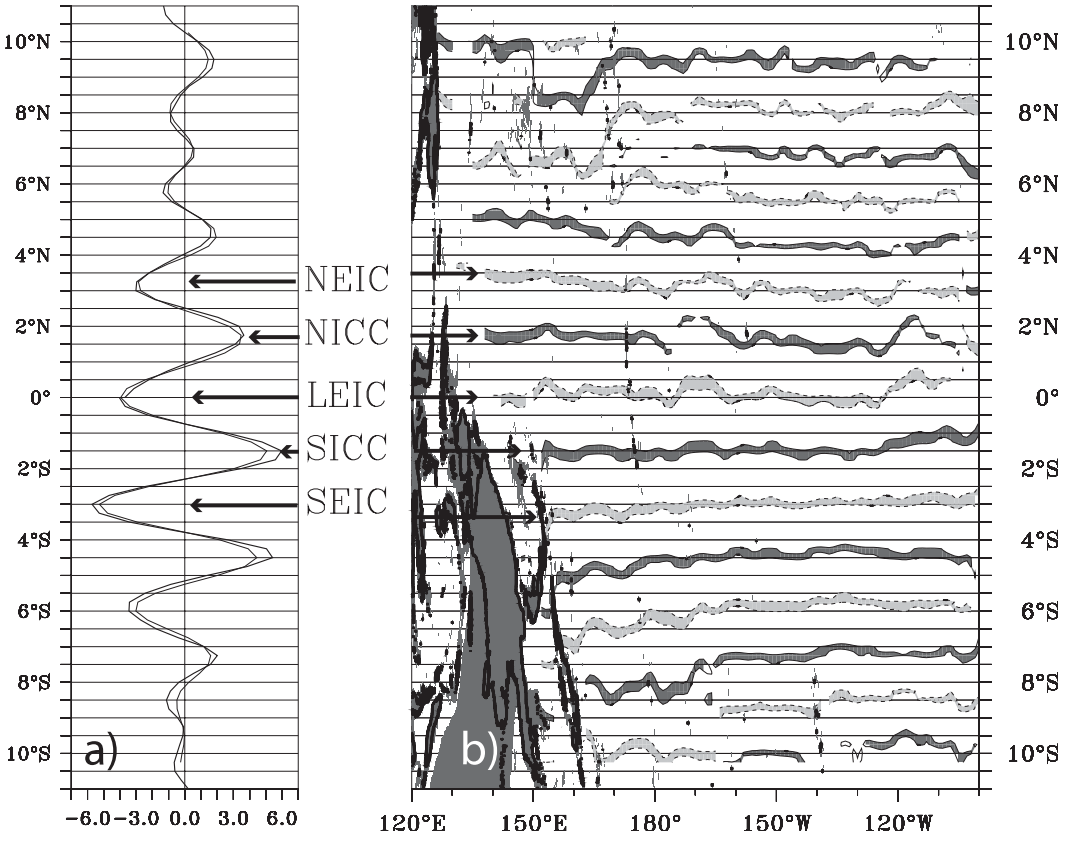

FIG. 3. (left) Mean zonal current u at 1000 m in cm s^{-1}, zonally averaged in the 160°E–120°W band in the Southern Hemisphere and in the 120°E–120°W band in the Northern Hemisphere. Thick lines are the gridded u, and thin lines are the reconstruction from CD. (right) Positions of the CD-reconstructed zonal jets. Eastward jets are in dark gray; westward jets are in light gray.

In the Southern Hemisphere, the SEIC flows westward at 3°S (3.5°S in the western Pacific) from about 90°W to New Ireland. As with the SICC, its mean amplitude of 6 cm s^{-1} is zonally constant. Three other jets are also visible in the Southern Hemisphere: eastward along 4.5°S, westward along 6°S, and eastward along 7°–7.5°S. An additional westward jet along 8.5°S is weaker (only 2 cm s^{-1}) and only present in the central part of the basin, from 110° to 160°W.

In the Northern Hemisphere, the NEIC flows westward at 3°N (3.5°N in the western Pacific) from about 105°W to the western coast (Fig. 2). Along 4.5°N, a weak eastward current is observed. Farther poleward, the currents are blurred in the western Pacific (Fig. 4a), but alternating eastward and westward jets are visible from east of the date line to about 110°W, flowing along 5.5°, 7°, 8°, and 9.5°N. To the best of our knowledge, these jets poleward of 3° have never been observed or described, except individually during synoptic cruises.

Although the overall impression suggests a simple series of alternating jets, some irregularities are evident: the jets are not perfectly symmetrical about the equator and the northern jets are weaker than their southern counterparts. All the jets also appear to slant slightly away from the equator in the western part of the basin. To quantify these observations, maps of local amplitude and meridional wavelength of the jets obtained from complex demodulation are shown in Figs. 4b,c. They confirm that the amplitude of the jets is stronger in the Southern Hemisphere and the western part of the northern tropical Pacific. The meridional wavelength map (Fig. 4c) corroborates the visual impression that the latitudinal distance between the jets increases from east to west; in the central Pacific, the wavelength is close to 2.75° in the Southern Hemisphere and close to 2.25°–2.5° in the Northern Hemisphere. In the western Pacific, the wavelength is larger, close to 3.25°–3.5°.

These analyses suggest that there are at least two regions (the western Pacific and the central–eastern Pacific) where the characteristics of the jets are somewhat different. This will be further discussed in section 4.

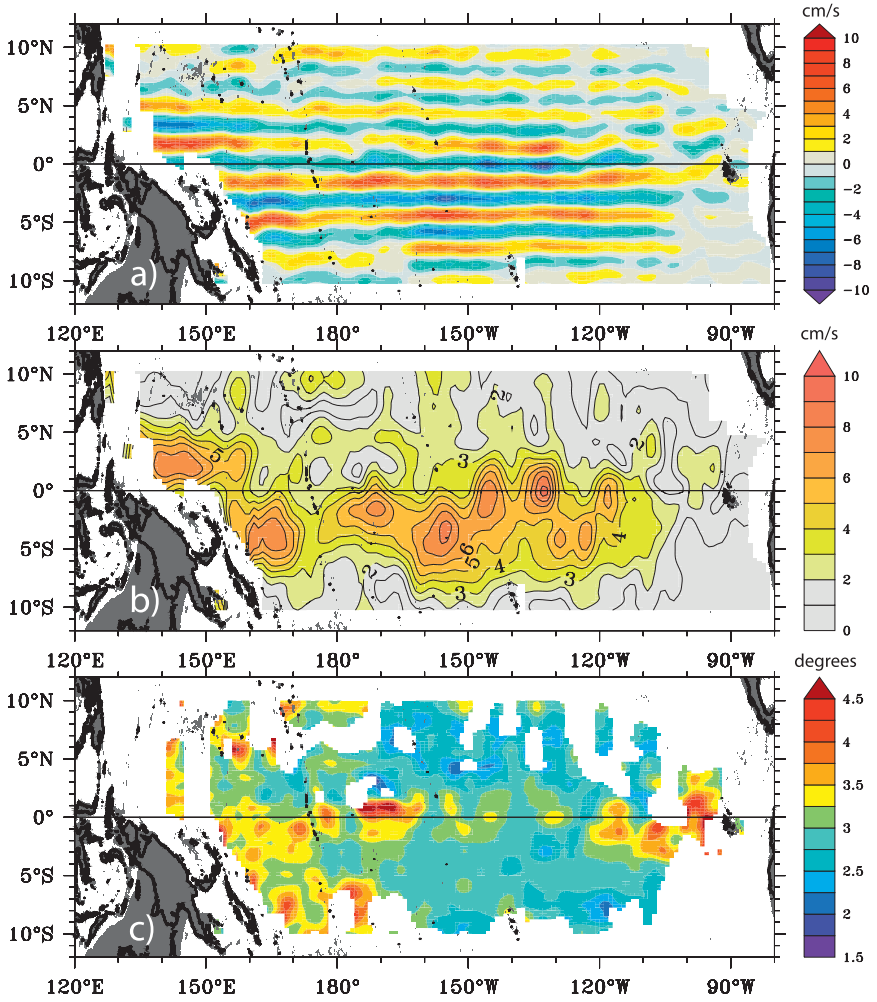

FIG. 4. Result of CD of the mean zonal current at 1000 m, showing (a) the reconstructed filtered currents (cm s^{-1}); (b) amplitude of the demodulated signal (cm s^{-1}); and (c) local meridional wavelength (degrees of latitude). Topography shallower than 1000-m depth is shaded in dark gray.

b. Zonal jets at 1500 m

Figure 2b shows the mean zonal currents at 1500 m. As seen in Fig. 1b, floats drifting at 1500 m are less numerous and large areas remain unsampled. Nevertheless, Fig. 2b gives interesting clues about the deeper extension of the zonal jets.

Alternating eastward/westward zonal jets are also present at 1500 m and appear, at first glance, to have a similar geographical distribution than the ones observed at 1000 m. This suggests that the jets have a large vertical extension, and that currents at 1000 and 1500 m are connected. Subtle differences may, however, be noticed: in the southwestern region, where they are well resolved, the jets at 1500 m are slightly closer to the equator than they are at 1000 m. The southwestern jets are centered at 6°, 7.5°, and 9.5°S instead of 6.6°, 8.5°, and 10°S, as they are in the east. The 1500-m jets also appear to be stronger poleward of 7°S and weaker equatorward of 7°S than at 1000 m. However, more observations would be needed to confirm these preliminary results.

It is also worth noting that currents at 1500 m are westward along the equator, as at 1000 m. This is surprising, because it is known that, at these depths, equatorial deep jets alternating in the vertical with a wavelength of several hundred meters are present (Firing et al. 1998, their Fig. 1). On the other hand, their figure shows westward currents at 1000 and 1500 m, in agreement with our observations, with one westward current and two eastward currents between these two depths. Thus, the similarity between 1000- and 1500-m zonal currents at the equator is probably coincidental. Off the equator, observations of extra-equatorial jets are sparse but do not suggest the existence of vertically alternating deep jets. Synoptic observations

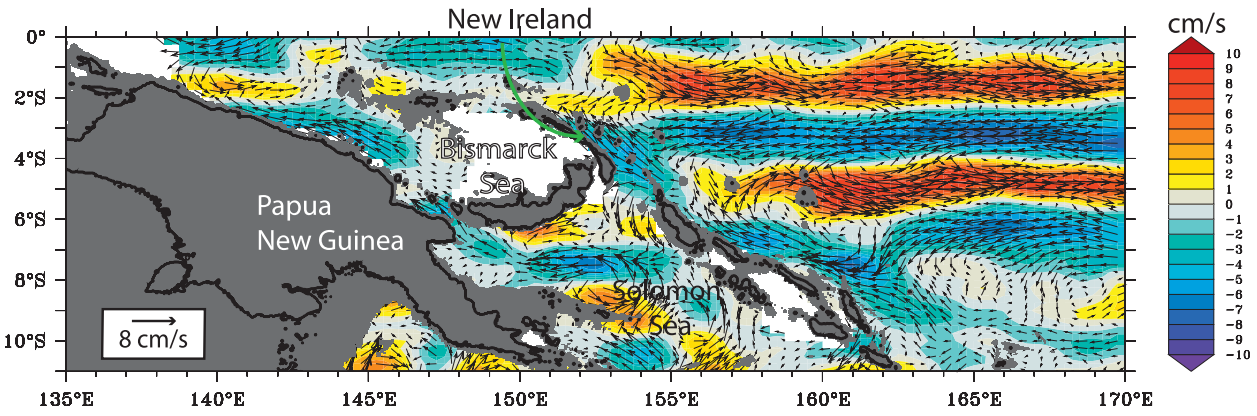

FIG. 5. Mean 1000-m zonal and meridional currents (cm s^{-1}; vectors) in the southwest tropical Pacific. Colors represent the mean zonal current (scale at right). Topography shallower than 1000-m depth is shaded in dark gray. White areas (as in Bismarck Sea) are locations with no data.

(Firing et al. 1998) revealed mostly weak vertical shear between 1000- and 1500-m currents off the equator, consistent with the present observations that show similarity of zonal jets at 1000 and 1500 m off the equator.

c. *Connection to the western boundary currents*

Figure 5 shows the mean 1000-m zonal and meridional velocities near the southwestern boundary, constituted by Papua New Guinea, New Ireland, and the Solomon Island chain, east of the Solomon Sea. The picture is qualitatively similar at 1500 m (not shown).

Interestingly, all the zonal jets originate very close to the coast. Because the decorrelation scale of the optimal interpolation is 110 km near the coast, this is not an artifact of the gridding. The SICC along 1.5°–2°S is fully developed within 300 km of the New Ireland coast but appears to also be present near the coast of mainland New Guinea at 143°E, despite the topographic barriers. This is consistent with observational and numerical results of Zenk et al. (2005), who also observed a SICC at 142°E, within the Bismarck Sea. The other eastward jets at 5° and 8.5°S (more clearly at 1500 m, where this jet is stronger; not shown) also originate only a few degrees east of the coast. Mean meridional velocities indicate that each eastward jet appears to be fed by waters coming from both adjacent westward jets. In the same way, each westward jet appears to feed both its southern and northern adjacent eastward jets. Along the Solomon Islands and New Ireland, the 1000-m mean boundary current is mostly northward, 100–200 km wide, confirming preliminary results from Davis (1998, 2005); flow at these depths is westward—into the Solomon Sea—through the two straits deep enough to let water in (Solomon Strait at 5°S, 153°E and Indispensable Strait at 10°S, 161°E).

In the Northern Hemisphere (not shown), sampling near the western coast is not sufficient to resolve analogous western boundary connections between the jets, if they exist (Fig. 1), and eddies appear to dominate the mean flow, similar to the conclusions from Firing et al. (2005). There are however indications of northward flow to 5°N. The NICC originates a few degrees east of Halmahera coast, fed by flow originating from the LEIC or from the New Guinea Coastal Undercurrent at intermediate levels, after circulating around the Halmahera eddy, and also by waters from the NEIC turning southeastward between 130° and 140°E. These results are also consistent with Zenk et al. (2005). North of 5°N, no clear circulation could be deduced.

d. *Seasonal variability*

It is not possible to resolve the full temporal structure of the jets' variability, given the sampling and the short record spanning only a few years. However, it is possible to characterize their seasonal variability.

Figure 6 shows the 1000-m zonal velocity anomalies at the equator and at 4°N and 4°S (left panels). At the three latitudes, an annual cycle of zonal velocity is evident. Current anomalies are out of phase between the equator and 4° and propagate westward at a speed of about 0.45 m s^{-1}. This is consistent with the vertical propagation of an annual Rossby wave (Lukas and Firing 1985; Kessler and McCreary 1993; Marin et al. 2010). Along the Rossby wave path deduced from linear regression, zonal velocity anomalies are averaged in a 3-month running window (between the black lines shown in Fig. 6, left), and the resulting meridional structure is shown in the right panel (black continuous line). We also computed the first annual harmonic of the zonal currents and then extracted it along the paths shown in Fig. 6. The

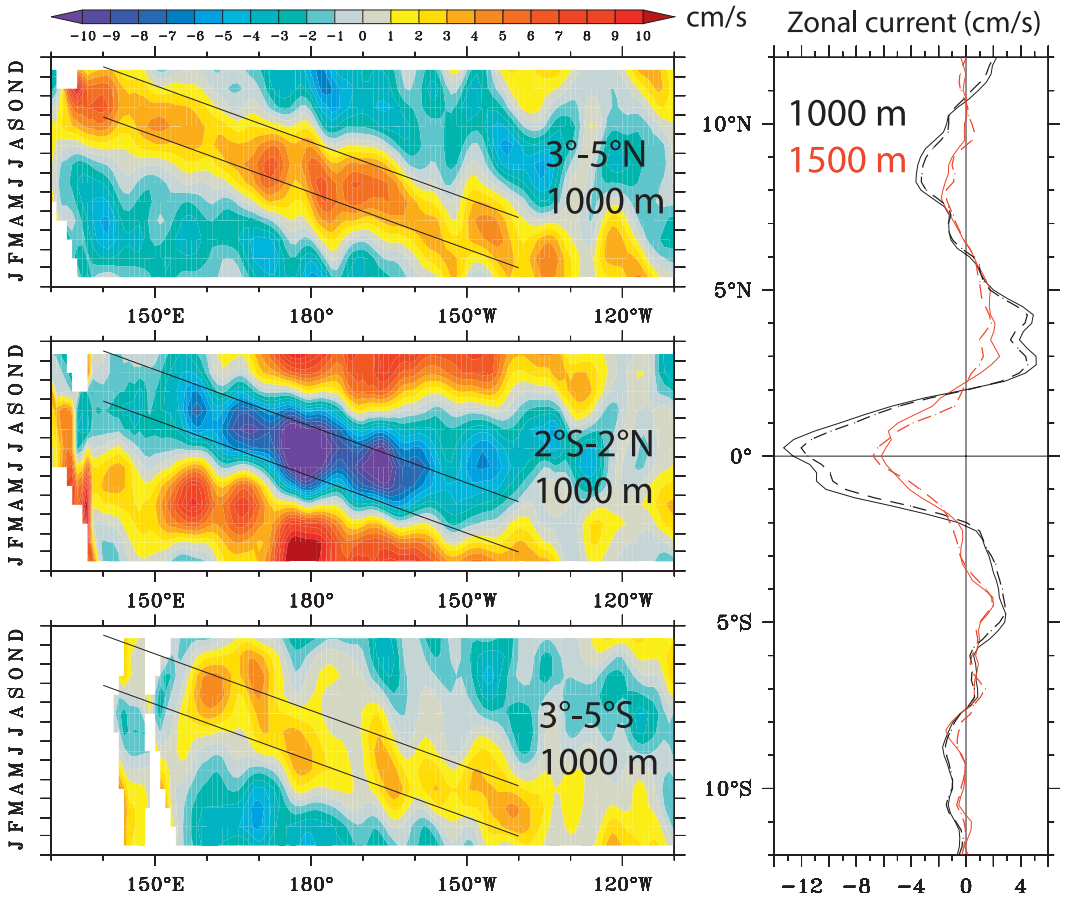

FIG. 6. (left) Seasonal anomalies (mean removed) of 1000-m zonal currents (cm s^{-1}) averaged between (top) 3°–5°N, (middle) 2°S–2°N, and (bottom) 3°–5°S. (right) Zonal velocity anomalies averaged along the paths shown in the left panels (in black lines), between 160°E and 160°W, for 1000-m current anomalies (thin black) and their first annual harmonic (dashed black). The same calculations have been made for zonal current anomalies at 1500-m currents, and 1500-m zonal currents anomalies and their first annual harmonic have been averaged along similar Rossby paths, shifted one month in advance (red thin and dashed lines).

harmonic's meridional structure (Fig. 6, right, black dashed line) is almost identical to that of the raw data, confirming that the seasonal variability is largely at 1 cycle per year.

Interestingly, the zonal currents' seasonal variability exhibits a meridional scale quite different from that of the mean currents, with a meridional wavelength of 7°–9° instead of 3°. The zonal currents' annual variability is thus superimposed on the mean zonal jets, but the scale difference suggests that the seasonal dynamics are distinct from the background zonal jets' dynamics. The amplitude of zonal current anomalies is maximum at the equator (about 12 cm s^{-1}). Local maxima of opposite sign are seen at 4°–5°, and then secondary positive maxima are seen at 8°–9°. This suggests that more than one meridional Rossby mode are present and in particular that the third meridional mode is likely to be important. It is also worth noting that anomalies are not perfectly symmetrical with respect to the equator: they are stronger in the Northern Hemisphere, consistent with the upper ocean observations of Perez et al. (2005), who demonstrated that this asymmetry was linked to meridional shear of the equatorial current system.

A plot analogous to Fig. 6a was produced for the 1500-m zonal currents (not shown). The results were similar, with the 1500-m zonal anomalies also propagating westward slightly advanced in phase (about one month or less) than the 1000-m zonal current anomalies. Along this time-shifted Rossby wave path, the 1500-m zonal velocity anomalies were also averaged in a 3-month window, and their meridional structure is superimposed in red in Fig. 6b. Though weaker, the meridional structure of the 1500-m current anomalies is similar.

How does this seasonal variability change the zonal jets? At the equator, seasonal anomalies are larger than the mean current, implying a seasonal reversal of the LEIC, consistent with the synoptic observations of Gouriou et al. (2006). Off the equator, anomalies are weaker (2–6 cm s^{-1}) and have similar amplitude to the mean currents. They do not lead to annual current reversals in the Southern Hemisphere, where the mean currents exceed the annual anomalies, but do suggest cancellation or weak seasonal reversal of the zonal currents in the Northern Hemisphere. Therefore, it appears that the southern jets should be discernible during any season, whereas the northern jets disappear seasonally and are clearly discernible only in the annual mean, not in monthly means.

This is not the first time that a downward-propagating Rossby wave has been seen in observations (e.g., Lukas and Firing 1985; Kessler and McCreary 1993). However, to our knowledge, it is the first time that in situ velocity observations with basinwide coverage confirm the existence of such a wave, with all its expected characteristics. The phase and amplitude of the currents' seasonal variability is consistent with the numerical results of Marin et al. (2010, their Fig. 10), which were themselves consistent with Kessler and McCreary's (1993) vertical isotherm displacement observations. Marin et al. (2010) found that the currents' seasonal variability amplitude ranged from 10 to 20 cm s^{-1} at the equator at 1000 m, with a maximum at 180°, and from 6 to 10 cm s^{-1} at 1500 m. The phase was seen to propagate upward, and at 180° the zonal current was maximum in January (December) and minimum in July (June) at 1000 m (1500 m). Our results show that the currents' seasonal variability amplitude is about 12 cm s^{-1} at the equator at 1000 m, with a maximum at 180°, and about 7 cm s^{-1} at 1500 m. The phase difference between these two depths is consistent with upward phase propagation. This agreement with previous observations and models of the zonal currents seasonal cycle gives us confidence in our data and gridding procedure.

4. Discussion

We have presented maps of observed zonal jets at 1000 and 1500 m in the tropical Pacific Ocean, based on Argo float subsurface velocities. At both depths, a series of alternating zonal jets with a meridional scale of about 1.5° was seen flowing across the basin over 10°S–10°N. Explaining the dynamics of these jets is beyond the scope of this study. Several theories have been proposed to explain the existence of the so-called extra-equatorial jets (d'Orgeville et al. 2007; Hua et al. 2008; Menesguen et al. 2009; Ascani et al. 2010), which invoke the destabilization or the dissipation of equatorial mixed Rossby–gravity waves that rectify into mean zonal flow. However, these theories are tied to the meridional scale of these waves and thus have only focused on the generation of the near-equatorial deep jets: that is, on the SICC and the NICC between 3°S and 3°N. Our observations reveal that the SICC and NICC are embedded into a broader system of zonal jets; it is thus not clear if these zonal jets can be considered as a purely equatorially trapped phenomenon, as has been usually assumed in connection with previous observations of the near-equatorial jets described in the literature. If in fact the entire 2000-km-wide jet region is a connected whole, then the individual elements become less significant, and the confusing edifice of historical names (LEIC, SICC, NICC, SEIC, NEIC, etc.), implying that these are discrete, independent features, may be inappropriate.

One possible mechanism would be an extension of the above equatorial theories (that involve only the most equatorially trapped waves), to a broader spectrum of waves, particularly those with larger meridional scales. Alternatively, these jets could be seen as part of the planetary zonal jets system observed in every part of the World Ocean (Maximenko et al. 2005; Nakano and Hasumi 2005; Melnichenko et al. 2010). In that case, a possible mechanism would be that these jets are generated by geostrophic turbulence on a beta plane (Richards et al. 2006).

The question is still open, and we hope that the observations presented here will stimulate both theoretical and modeling studies to elucidate the dynamics responsible for these jets. Indeed, the jets' characteristics, described in section 3a, give new hints on the properties of the jets and raise a number of questions:

- Why are the northern jets weaker, blurred, and broken in several segments? Figure 1a indicates that the sampling is roughly equivalent in the Northern and Southern Hemispheres. Are the northern jets just shallower or less barotropic and thus inadequately sampled by the Argo float trajectories at 1000 m? On the other hand, is there a theoretical reason inherent to the differences in the hemispheres (e.g., linked to the structure of the mean thermocline or to the bathymetry)?
- Why are the jets stronger in the western part of the basin, and how do they disappear in the eastern part of the basin?
- Why does the meridional wavelength of the jets change from east to west? Why are they apparently slanted slightly away from the equator in the western part of the basin? In the map of jet maxima (Fig. 3b), it is not clear if this change is gradual or instead steplike. If the apparently increased separation in the west is steplike

and linked to topographic barriers, it is possible that the meridional wavelength of the jets is different in separated topographic basins and that zonal jets are generated independently in each basin. Their connection from west to east, as well as their zonal coherence across the basin, more clearly seen near the equator and in the south, might be coincidental. This would corroborate the conclusions of Maximenko et al. (2005), who noted that zonal jets are seen in isolated basins and that their widths differ from place to place.

We have presented maps of the mean Eulerian currents. When looking at the full trajectory of individual floats, the Lagrangian picture is somewhat different. In the mean, the meridional velocity is close to zero, but most of the floats individually have significant meridional velocities and change latitudes often, joining one jet after another. Because the Argo floats spend some time at the surface, their surface drift obscures the Lagrangian view of subsurface velocities. It is thus hazardous to draw conclusions on the middepth jet characteristics from individual float trajectories: are these jets laminar flows forming large-scale closed circulations or do they result from a long-term time average of small-scale recirculations and/or eddy-like motions? This may have important implications for the transport, as well as mixing, of water masses and tracers by the jets.

Acknowledgments. This study strongly relies on Argo data subsurface drifts. Argo float data were collected and made freely available by the International Argo Program and the national programs that contribute to it. The Argo Program is part of the Global Ocean Observing System. The authors thank two anonymous reviewers for their comments, especially on theoretical aspects, which helped to clarify the discussion. The authors also wish to acknowledge use of the Ferret program for analysis and graphics in this paper. Ferret is a product of NOAA's Pacific Marine Environmental Laboratory. (Information is available at http://ferret.pmel.noaa.gov/Ferret.) This work is cofunded by ANR Project ANR-09-BLAN-0233-01 and INSU/LEFE Project IDAO; it is a contribution to the CLIVAR/SPICE International Program (http://www.clivar.org; http://www.solomonseaoceanography.org).

REFERENCES

Ascani, F., E. Firing, P. Dutrieux, J. P. McCreary, and A. Ishida, 2010: Deep equatorial ocean circulation induced by a forced–dissipated Yanai beam. *J. Phys. Oceanogr.,* **40,** 1118–1142.

Bloomfield, P., 1976: *Fourier Decomposition of Time Series: An Introduction*. John Wiley, 258 pp.

Condie, S. A., and J. R. Dunn, 2006: Seasonal characteristics of the surface mixed layer in the Australasian region: Implications for primary production regimes and biogeography. *Mar. Freshwater Res.,* **57,** 569–590.

Davis, R. E., 1998: Preliminary results from directly measuring middepth circulation in the tropical and South Pacific. *J. Geophys. Res.,* **103** (C10), 24 619–24 639.

——, 2005: Intermediate-depth circulation of the Indian and South Pacific Oceans measured by autonomous floats. *J. Phys. Oceanogr.,* **35,** 683–707.

De Mey, P., and Y. Menard, 1989: Synoptic analysis and dynamical adjustment of GEOS-3 and Seasat altimeter eddy fields in the northwest Atlantic. *J. Geophys. Res.,* **94** (C5), 6221–6231.

d'Orgeville, M., B. L. Hua, and H. Sasaki, 2007: Equatorial deep jets triggered by a large vertical scale variability within the western boundary layer. *J. Mar. Res.,* **65,** 1–25.

Firing, E., 1987: Deep zonal currents in the central equatorial Pacific. *J. Mar. Res.,* **45,** 791–812.

——, S. E. Wijffels, and P. Hacker, 1998: Equatorial subthermocline currents across the Pacific. *J. Geophys. Res.,* **103** (C10), 21 413–21 423.

——, Y. Kashino, and P. Hacker, 2005: Energetic subthermocline currents observed east of Mindanao. *Deep-Sea Res. I,* **52** (3–4), 605–613.

Gouriou, Y., T. Delcroix, and G. Eldin, 2006: Upper and intermediate circulation in the western equatorial Pacific Ocean in October 1999 and April 2000. *Geophys. Res. Lett.,* **33,** L10603, doi:10.1029/2006GL025941.

Hua, B. L., M. d'Orgeville, M. D. Fruman, C. Menesguen, R. Schopp, P. Klein, and H. Sasaki, 2008: Destabilization of mixed Rossby gravity waves and the formation of equatorial zonal jets. *J. Fluid Mech.,* **610,** 311–341.

Johnson, G. C., E. Kunze, K. E. McTaggart, and D. W. Moore, 2002: Temporal and spatial structure of the equatorial deep jets in the Pacific Ocean. *J. Phys. Oceanogr.,* **32,** 3396–3407.

Kessler, W. S., and J. P. McCreary, 1993: The annual wind-driven Rossby wave in the subthermocline equatorial Pacific. *J. Phys. Oceanogr.,* **23,** 1192–1207.

——, M. J. McPhaden, and K. M. Weickmann, 1995: Forcing of intraseasonal Kelvin waves in the equatorial Pacific. *J. Geophys. Res.,* **100** (C6), 10 613–10 631.

Lukas, R., and E. Firing, 1985: The annual Rossby wave in the central equatorial Pacific Ocean. *J. Phys. Oceanogr.,* **15,** 55–67.

Marin, F., E. Kestenare, T. Delcroix, F. Durand, S. Cravatte, G. Eldin, and R. Bourdalle-Badie, 2010: Annual reversal of the equatorial intermediate current in the Pacific: Observations and model diagnostics. *J. Phys. Oceanogr.,* **40,** 915–933.

Maximenko, N. A., B. Bang, and H. Sasaki, 2005: Observational evidence of alternating zonal jets in the world ocean. *Geophys. Res. Lett.,* **32,** L12607, doi:10.1029/2005GL022728.

Melnichenko, O. V., N. A. Maximenko, N. Schneider, and H. Sasaki, 2010: Quasi-stationary striations in basin-scale oceanic circulation: Vorticity balance from observations and eddy-resolving model. *Ocean Dyn.,* **60,** 653–666.

Menesguen, C., B. L. Hua, M. D. Fruman, and R. Schopp, 2009: Dynamics of the combined extra-equatorial and equatorial deep jets in the Atlantic. *J. Mar. Res.,* **67,** 323–346.

Nakano, H., and H. Hasumi, 2005: A series of zonal jets embedded in the broad zonal flows in the Pacific obtained in eddy-permitting ocean general circulation models. *J. Phys. Oceanogr.,* **35,** 474–488.

Ollitrault, M., M. Lankhorst, D. Fratantoni, P. Richardson, and W. Zenk, 2006: Zonal intermediate currents in the equatorial Atlantic Ocean. *Geophys. Res. Lett.,* **33,** L05605, doi:10.1029/2005GL025368.

Park, J. J., K. Kim, B. A. King, and S. C. Riser, 2005: An advanced method to estimate deep currents from profiling floats. *J. Atmos. Oceanic Technol.,* **22,** 1294–1304.

Perez, R. C., D. B. Chelton, and R. N. Miller, 2005: The effects of wind forcing and background mean currents on the latitudinal structure of equatorial Rossby waves. *J. Phys. Oceanogr.,* **35,** 666–682.

Richards, K. J., N. A. Maximenko, F. O. Bryan, and H. Sasaki, 2006: Zonal jets in the Pacific Ocean. *Geophys. Res. Lett.,* **33,** L03605, doi:10.1029/2005GL024645.

Rowe, G. D., E. Firing, and G. C. Johnson, 2000: Pacific equatorial subsurface countercurrent velocity, transport, and potential vorticity. *J. Phys. Oceanogr.,* **30,** 1172–1187.

Zenk, W., G. Siedler, A. Ishida, E. Holfort, Y. Kashino, Y. Kuroda, T. Miyama, and T. J. Muller, 2005: Pathways and variability of the Antarctic Intermediate Water in the western equatorial Pacific Ocean. *Prog. Oceanogr.,* **67** (1–2), 245–281.